Microcavity organic laser device under electrical pumping

Xingyuan Liu,* Huibin Li, Chunyan Song, Yaqin Liao, and Miaomiao Tian

Laboratory of Excited State Processes, Changchun Institute of Optics, Fine Mechanics, and Physics, Chinese Academy of Sciences, Changchun 130033, China
**Corresponding author: holiday00017@mail.jl.cn*

Received November 17, 2008; revised December 24, 2008; accepted December 27, 2008; posted January 12, 2009 (Doc. ID 104225); published February 12, 2009

Lasing action in an electrically pumped organic laser device is demonstrated with a high quality factor (Q) microcavity structure formed by two high-reflective and low-loss electrical contacts. A 4-(dicyanomethylene)-2-*i*-propyl-6-(1,1,7,7-tetramethyljulolidyl-9-enyl)-4*H*-pyran-doped tris(8-hydroxyquinoline)aluminum (Alq_3) film serves as the active layer. A single longitudinal lasing cavity mode is obtained at 621.7 nm with a threshold current density of 860 mA/cm^2 under a room temperature pulse operation.

OCIS codes: 140.3948, 140.2020, 160.4890.

Organic semiconductor materials have been successfully used in many optoelectronic devices including organic light-emitting devices (OLEDs) [1], field-effect transistors [2], solar cells [3], and optically pumped lasers [4–9]. Much improvement has been shown in realizing electrically pumped organic laser devices (OLDs) [10–15]. Highly directional and coherence characteristics have been observed at electrically excited tandem OLEDs [14,15]. The major challenges are low carrier mobilities of organic films together with additional losses owing to contacts, carrier absorption, and other nonradiative mechanisms [5,6], which limit the thickness of organic films to thin layers and introduces serious optical losses in a waveguide or distributed-feedback structure [4,7].

One promising structure for electrically pumped OLDs is a microcavity that is formed by depositing one or multilayer organic materials between two mirrors (either dielectric stacks or metallic) separated by a few hundred nanometers [7,9]. A microcavity can modify the spontaneous emission properties of the materials inside spatially and spectrally owing to the alteration of the optical mode density within it. As a consequence, the interaction between material and light within the microcavity was changed greatly compared with the condition of free space [16]. In this Letter, we demonstrate an electrically pumped OLD with a high-Q microcavity structure.

As shown in Fig. 1(a), the electrically pumped OLDs are based on a half-wave microcavity structure: glass/bottom mirror (including anode)/MoO_3 (1 nm, anode buffer layer)/4,4′,4″-tris(*N*-naphthyl-*N*-phenylamino)triphenylamine (2T-NATA, 20 nm, hole injection layer)/*N*,*N*′-bis(3-naphthalen-2-yl)-*N*,*N*′-bis(phenyl)benzidine (NPB, 66 nm, hole transport layer)/2 wt. % 4-(dicyanomethylene)-2-*i*-propyl-6-(1,1,7,7-tetramethyljulolidyl-9-enyl)-4*H*-pyran (DCJTI)-doped Alq_3 (40 nm, active layer)/3-(4-biphenylyl)-4-phenyl-5-(4-tert-butylphenyl)-1,2,4-triazole (TAZ) (15 nm, exciton barrier layer)/Alq_3 (35 nm, electron transport layer)/LiF (1 nm, cathode buffer layer)/top mirror (including cathode). An indium vanadium oxide (IVO) film [17] and an Al film

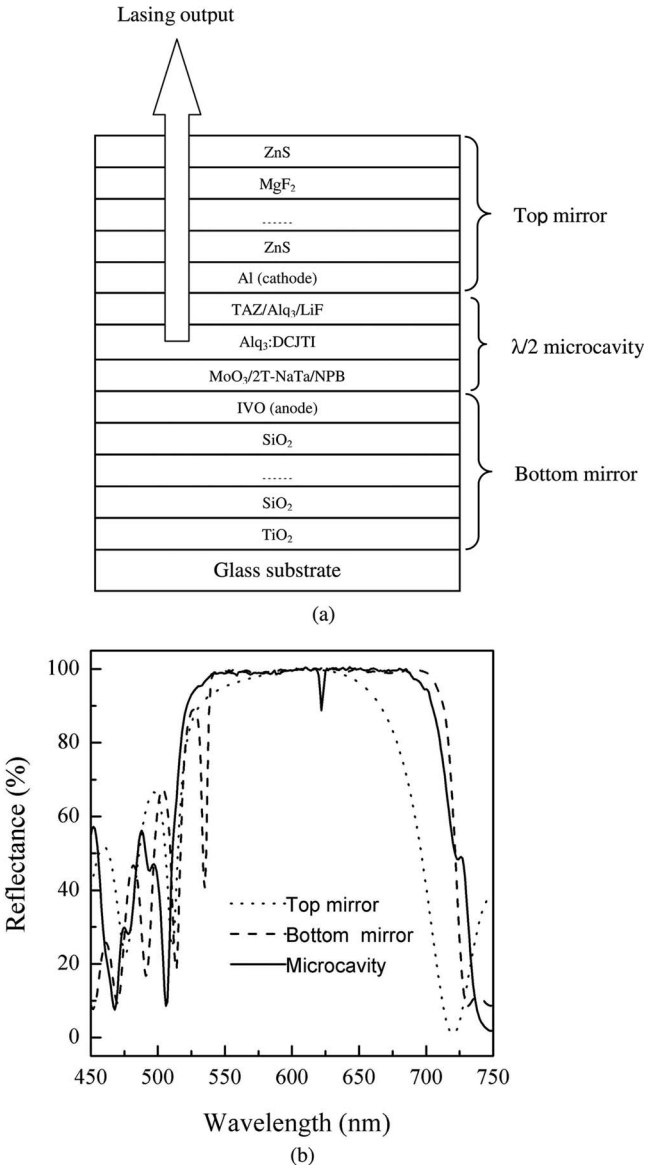

Fig. 1. (a) Schematic of the microcavity laser. (b) Measured reflectance spectra of top mirror, bottom mirror, and microcavity.

0146-9592/09/040503-3/$15.00

were used as the anode and the cathode, respectively. To reduce the absorption from the electrodes, the anode and the cathode were designed to be a composing part of the bottom mirror and the top mirror, respectively. The top mirror consisted of 10-nm-thick Al and a distributed Bragg reflector (DBR) structure of 7.5 pairs of ZnS/MgF_2 quarter-wave layers with a Bragg wavelength of 612 nm. The bottom mirror consisted of 71-nm-thick IVO film and a DBR structure of ten pairs of TiO_2/SiO_2 quarter-wave layers with a Bragg wavelength of 622 nm. The overall thickness of organic layers was selected to form a $\lambda/2$ laser cavity with the active layer situated around the antinode and the two organic layer/electrode interfaces located near the node of the confined cavity electromagnetic field at λ. Such a design can lower the optical absorption at a lasing wavelength from the electrodes and greatly enhance the cavity effect of the emission.

The TiO_2, SiO_2, and IVO layers were deposited by electron beam evaporation at a substrate temperature of 250°C in an oxygen pressure of 2×10^{-2} Pa. Metal and organic films were grown by thermal evaporation in a vacuum of 5×10^{-4} Pa. The ZnS and MgF_2 layers were deposited in a vacuum of 1×10^{-3} Pa by electron beam evaporation. All organic layers, ZnS, and MgF_2 layers were deposited with a substrate temperature of 80°C. For pulsed operation a Keithley 2430 was used to provide a pulse width of 0.2 ms and a duty ratio of 20%. Typical active areas had a diameter of 150 μm. The electroluminescence emission and reflectance spectra were measured with an Avantes fiber optic spectrometer (spectral resolution of 0.04 nm) normal to the OLD surface. All measurements were performed in air at room temperature.

The measured reflectance spectra of the top mirror and the bottom mirror are shown in Fig. 1(b). It shows that the maximum reflectance of the two mirrors are greater than 99% around 622 nm, which means that a minimum absorptance of less than 1% can be obtained at the same wavelength. The transmission "dip" in the microcavity reflectance spectra at 622 nm corresponds to the effective cavity mode. Figure 2 shows the emission spectra of the OLD measured with a 14° full-angle acceptance cone. The inset shows that the Alq_3:DCJTI film has a wide photoluminescence (PL) emission spectrum with the peak at about 620 nm. The stimulated emission cross section of the active material is about 7.8×10^{-16} cm^2. The spontaneous emission spectrum below threshold was modified by microcavity effects. The main peak at 621.7 nm is the cavity resonance mode with a FWHM of 2.62 nm, which corresponds to a cavity quality factor $Q=237$. The dependence of the spectral peak intensity on the current density in Fig. 3 indicates a clear laser threshold (J_{th}) at 860 mA/cm^2, above which a sharp increase in output intensity has been observed. The voltage at J_{th} is about 25 V. Increasing the current density leads to a decrease of the FWHM to 2.10 nm at J_{th} and 1.95 nm at 1.47 J_{th}.

The collimated circularly symmetric output beam was observed from the top side along the axis normal

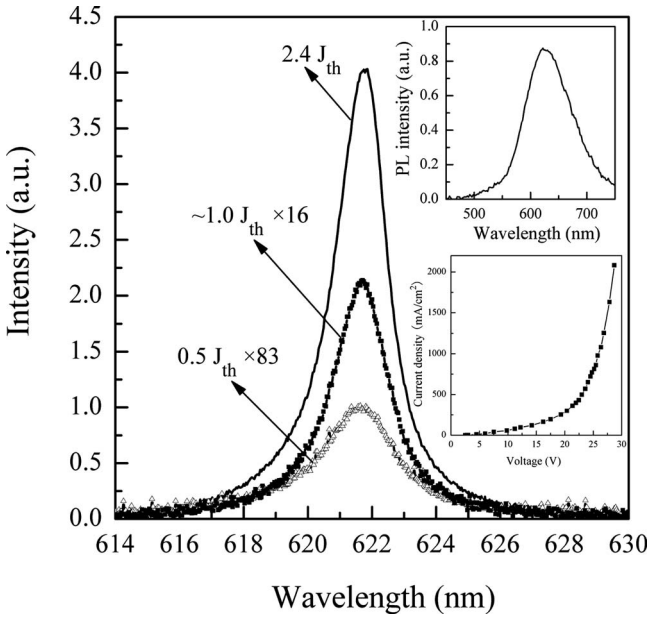

Fig. 2. Emission spectra under a different current density; the two insets show the PL emission spectrum of Alq_3:DCJTI film and I-V characteristic of the device.

to the cavity. One of the fundamental properties of the laser is its ability to produce spatially coherent beams. The coherence of the beam was determined by conventional Young's double-slit interferometry [18]. The output beam was focused onto the double slit directly. The slits are 60 μm wide, separated by 120 μm. The degree of coherence of the lasing is calculated from the fringe visibility V given by $(I_{max}-I_{min})/(I_{max}+I_{min})$ (where I_{max} and I_{min} are the maximum and minimum intensities). Figure 4(a) shows a typical double-slit interferogram. The calculated V below and above the threshold is 0.51 and 0.89, respectively. It indicates that the coherence from the OLD device is comparable with those of other types of lasers [14]. Beam parameters of the OLD device have been investigated by the Rayleigh method with a Beam Profiler 2320A [19]. Far-field beam profiles are shown in Fig. 4(b). The measured far-field full divergence angle below and above the threshold is 53 and 32 mrad, respectively. The times-diffraction-limit factor (M_2) is 13.

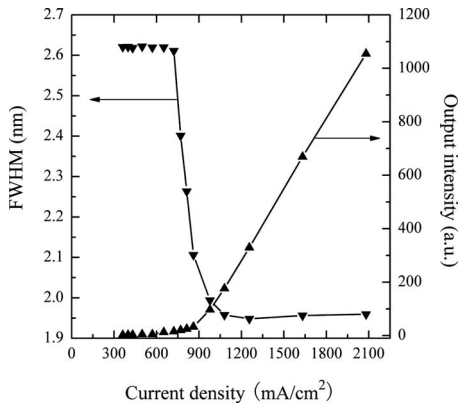

Fig. 3. FWHM and output intensity of the microcavity laser as a function of injection current density.

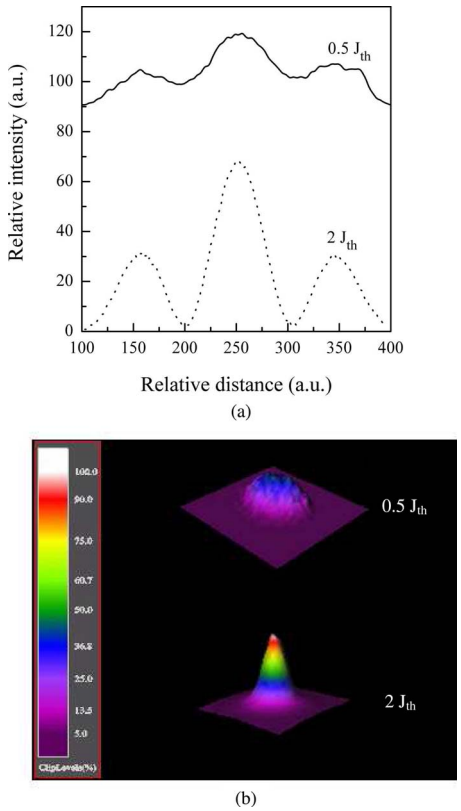

Fig. 4. (Color online) (a) Digital profile of the two-slit interference captured with a CCD camera below (solid curve) and above (dotted curve) threshold. (b) Far-field beam profiles below and above threshold.

The gain for the cavity mode must balance the overall optical losses to reach the threshold. In the OLD, the active layer belongs to a host-guest molecules system that has a minimized self absorption loss owing to effective Förster energy transfer. A high reflective cathode contact and an anode contact lead to a low mirror loss. Other losses, such as excited state absorption and triplet absorption belong to dipole–dipole interaction and can be modified by a strong cavity effect. Our results suggest that a suitable high-Q microcavity structure can improve the spontaneous emission rate and minimize optical losses, leading to a reduced threshold current density. The low threshold J_{th} in this Letter is consistent with the optically pumped experiment (the pumping source was a frequency-tripled Nd:YAG pulse laser with a repetition rate of 10 Hz and pulse duration of 1 ns) results that show a very low threshold of 0.35 nJ/cm^2 with a prediction of J_{th} below 1.0 A/cm^2. Normal OLEDs made by substituting ITO for the bottom mirror and Al for the top mirror show a balanced external quantum efficiency (EQE) of 5.8% under a different current density. EQE can be improved greatly by substituting IVO for ITO. Electroluminescent properties of OLED are important for realizing the laser.

The improvement in the OLD performance is feasible by the optimization of the laser structure and the fabrication process as well as the selection of suitable organic materials. This will bring a room-temperature cw laser. A surface-emitting microcavity structure facilitates the fabrication of electrically pumped OLDs in extremely small sizes and two-dimensional laser arrays, making them attractive for a wide range of applications including displays, optical communication, care diagnostics, and chemical sensors.

In conclusion, an electrically pumped surface-emitting organic laser device has been demonstrated in amorphous organic films with a microcavity structure. The high-quality factor and low optical loss microcavity is constructed by two high-reflective electrical contacts with a hybrid multiplayer structure of an electrode thin layer capped with DBR. The lasing peak is located at 621.7 nm with a threshold current density of 860 mA/cm^2 under a room temperature pulse operation mode. The laser beam has a far-field full divergence angle of 32 mrad and an M_2 factor of 13.

The authors acknowledge the financial support of the Chinese Academy of Sciences (CAS) Innovation Program, Jilin Province Science and Technology Research Project 20050108, and the National Natural Science Foundation of China (NSFC) under grants 60376029 and 10174077.

References

1. C. W. Tang and S. A. VanSlyke, Appl. Phys. Lett. **51**, 913 (1987).
2. D. J. Gundlach, Y. Y. Lin, T. N. Jackson, S. F. Nelson, and D. G. Schlom, IEEE Electron Device Lett. **18**, 87 (1997).
3. C. J. Brabec, N. S. Sariciftci, and J. C. Hummelen, Adv. Funct. Mater. **11**, 15 (2001).
4. M. D. McGehee and A. J. Heeger, Adv. Mater. **12**, 1655 (2000).
5. N. Tessler, J. Adv. Mater. **11**, 363 (1999).
6. M. A. Baldo, R. J. Holmes, and S. R. Forrest, Phys. Rev. B **66**, 035321 (2002).
7. V. G. Kozlov, V. Bulovic, P. E. Burrows, M. Baldo, V. B. Khalfin, G. Parthasarathy, and S. R. Forrest, J. Appl. Phys. **84**, 4096 (1998).
8. X. Liu, C. Py, Y. Tao, Y. Li, J. Ding, and M. Day, Appl. Phys. Lett. **84**, 2727 (2004).
9. T. W. Lee, O. O. Park, H. N. Cho, and Y. C. Kim, Opt. Mater. (Amsterdam, Neth.) **21**, 673 (2002).
10. C. Gärtner, C. Karnutsch, C. Pflumm, and U. Lemmer, IEEE J. Quantum Electron. **43**, 1006 (2007).
11. C. Gärtner, C. Karnutsch, U. Lemmer, and C. Pflumm, J. Appl. Phys. **101**, 023107 (2007).
12. C. Pflumm, C. Karnutsch, M. Gerken, and U. Lemmer, IEEE J. Quantum Electron. **41**, 316 (2005).
13. F. J. Duarte, Appl. Phys. B **90**, 101 (2008).
14. F. J. Duarte, Opt. Lett. **32**, 412 (2007).
15. M. Reufer, J. Feldmann, P. Rudati, A. Ruhl, D. Müller, K. Meerholz, C. Karnutsch, M. Gerken, and U. Lemmer, Appl. Phys. Lett. **86**, 221102 (2005).
16. H. Yokoyama, Science **256**, 66 (1992).
17. H. Li, N. Wang, and X. Liu, Opt. Express **16**, 194 (2008).
18. N. Negi, H. Yamamoto, Y. Hayasaki, and N. Nishida, Proc. SPIE **4416**, 384 (2001).
19. ISO 11146, Lasers and laser-related equipment—test methods for laser beam parameters—beam width, divergence, angle, and beam propagation factor (1999).